Self-potential Inversion for the Estimation of Permeability Structure

Yusuke Ozaki[1,2], Hitoshi Mikada[1], Tada-noti Goto[1] and Junichi Takekawa[1]
[1]Department of Civil and Earth Resources Engineering, Graduate School of Engineering, Kyoto University, Kyoto, Japan 615-8540
Email: ozaki.yusuke.57u@st.kyoto-u.ac.jp
[2]Japan Society for the Promotion of Science (JSPS) Research Fellow

ABSTRACT

The self-potential (SP) method is one geophysical method useful for estimating properties of groundwater flow. The effect of a permeability anomaly on a SP profile has been discussed in the literature, but neither the feasibility of using SP measurements to estimate the permeability structure nor the resolution of the inversion results of an SP profile have been given much attention. In this study, we developed a two-dimensional inversion code for the estimation of permeability structure. We applied this inversion to a synthetic SP profile on the ground surface affected by the permeability structure to evaluate the resolution of the SP inversion. Four models, which include a permeability anomaly located in the center of a slope, are used for the evaluation of the inversion performance. A priori data, including the distribution of the streaming current coefficient, electrical conductivity and flux volume at the discharge and recharge, are input to the inversion. A horizontal zone with high permeability and a vertical zone with low permeability can be reconstructed using the inversion. However, the horizontal low permeable zone and the vertical high permeable zone cannot be imaged clearly. The regional groundwater flow pattern around the permeability anomaly has a great effect on the SP pattern at the surface. For an accurate inversion of SP data, it is necessary that the inversion process consider the effect of flow pattern around the permeability anomaly on the SP profile.

Introduction

The self-potential or streaming potential (SP) method is one geophysical method useful for the estimation of groundwater flow because the presence of the SP is primarily generated by groundwater flow. Observed SP profiles have been related to direction of groundwater flow and analyzed qualitatively. Recently, several quantitative analysis methods of the SP profile have been developed to transform a SP profile to parameters related to groundwater flow; for example, the estimation of water table (Founier, 1989; Revil *et al.,* 2004), inversion of water head distribution (Sheffer, 2007; Jardani *et al.,* 2009), and inversion to estimate permeability (Jardani and Revil, 2009; Revil and Jardani, 2010).

Groundwater flow is affected by the subsurface permeability structure. The SP is susceptible to the groundwater flow pattern and the permeability structure (Sill, 1983; Titov *et al.,* 2002; Sheffer, 2007) because of its generation process. Our numerical simulations show that SP profiles reflect the regional groundwater flow pattern around a permeability anomaly (Ozaki *et al.,* 2012). From these features, it could be possible to estimate the spatial distribution of the permeability anomalies by analyzing the SP profile. However, considerations of the type of permeability anomalies, *e.g.,* shape or the combination of shape and permeability, and discussions of the resolution of the estimated permeability structure from a SP profile are limited in previous studies.

In this study, we developed a two-dimensional (2-D) inversion code for analyzing the water head distribution from the SP profile according to Sheffer (2007). We also developed a 2-D inversion code for analyzing the permeability structure from the distribution of the water head. We combined these two inversion codes and developed an inversion code for analyzing the permeability structure from a SP profile. The inversion is applied to synthetic data affected by subsurface permeability anomalies. We discuss the sensitivity of the SP profile to the permeability anomaly and the feasibility of the SP measurement to estimate the permeability structure.

Theory and Method

The governing equation for groundwater flow in the saturated zone is derived from Darcy's law and the mass conservation equation:

$$q = -\nabla(k\nabla h), \tag{1}$$

 DOI: 10.2113/JEEG19.3.193

where q is the external source of groundwater flow (s^{-1}), k is hydraulic permeability (m/s) and h is water head (m). When the source of subsurface electrical current caused by the groundwater flow is dominant and other sources are small enough to be negligible, the total subsurface electrical current is described by the sum of the conduction current and the convection current:

$$\boldsymbol{j} = -\sigma\nabla\varphi - l\nabla h, \tag{2}$$

where $\boldsymbol{j}$ is total subsurface electrical current density (A/m^2), σ is electrical conductivity (S/m), φ is electrical potential (V) and l is the streaming current coefficient (A/m^2). If the charge conservation of Eq. (2) is satisfied, then the water head and electrical potential are related:

$$\nabla(\sigma(\nabla\varphi)) = -\nabla(l\nabla h). \tag{3}$$

The effect of the electrical field on groundwater flow is negligible when the permeability is greater than about 10^{-8} m/s (Ishido and Pritchet, 1999; Revil *et al.,* 2003). To estimate the SP profile, we solved the water head distribution according to Eq. (1) and then solved the SP distribution according to Eq. (3) with the calculated water head distribution.

Finite element modeling substitutes the differential Eqs. (1) and (3) for the matrix and vector forms:

$$F_1(k)H = Q(k), \tag{4}$$

$$F_2(\sigma)\Phi = -F_3(l)H, \tag{5}$$

where F_1, F_2 and F_3 are matrices driven from the right side of Eq. (1), and left side and right side of Eq. (3), respectively, H is the water head vector, Q is a vector which represents the external source of groundwater flow and Φ is the electrical potential vector.

We define the objective function U according to the Tikhonov regularization. The objective function U is minimized by the permeability k for the inversion. The SP is related to the permeability through Eqs. (4) and (5):

$$\Phi = -F_2^{-1}(\sigma)F_3(l)F_1^{-1}(k)Q(k). \tag{6}$$

The objective function is described as:

$$U = \left\|\Phi_{obs} - (F_2^{-1}(\sigma)F_3(l)F_1^{-1}(k)Q(k))\right\|^2 + \lambda\|Cm\|^2 \tag{7}$$

where Φ_{obs} is an observed SP profile, λ is a hyper-parameter, C is the smoothness constraint matrix and $\boldsymbol{m}$ is log permeability.

In this study, we assume that both the electrical conductivity and the streaming current coefficient are independent of the permeability. The electrical conductivity and the streaming current coefficient are not modified in the iterative process. The Jacobian matrix of the SP data to the permeability becomes:

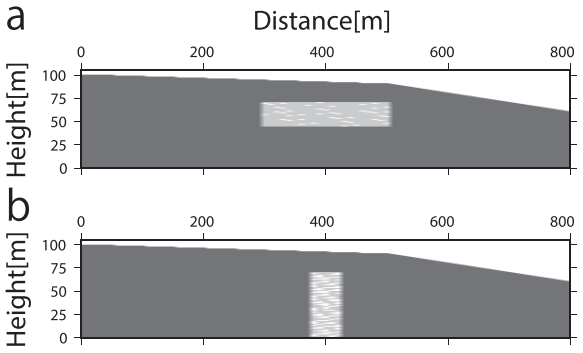

Figure 1. Permeability structures for the simulation models to calculate the SP profile for the inversion test. a) Horizontal anomaly model and b) vertical anomaly model.

$$\frac{\partial\Phi}{\partial k} = -F_2^{-1}(\sigma)F_3(l)\frac{\partial H}{\partial k}. \tag{8}$$

The optimal hyper-parameter is selected with the ABIC minimization method at every iterative step (Uchida, 1993). We modify the permeability structure with the Jacobian matrix as shown in Eq. (8), and the constraint matrix weighted with the optimal hyper-parameter.

Synthetic Data

In this study, we calculate the SP profile and input it as the observed data. Figure 1 shows permeability structure models for the calculation of input SP data. Two slope models with a permeability anomaly are used to calculate the test data for the inversion; one has a 200 m $\times$ 25 m horizontal permeability anomaly (Fig. 1(a)), and the other has a 40 m $\times$ 70 m vertical permeability anomaly (Fig. 1(b)). Two SP profiles are simulated for each slope model; one where the anomaly has a higher permeability than background, and the other where the anomaly has a lower permeability than background. To drive the groundwater flow, the water head values at the ground surface are assigned at the upstream and downstream boundaries of the models with a width of 50 m. The boundaries, except for the upstream/downstream areas, are set as a no-flow condition across the boundary. The calculation area of groundwater flow is discretized using a 10 m $\times$ 1 m square mesh. The model used for calculating the SP profile has a sufficiently larger scale than the model used for the groundwater calculation to satisfy the asymptotic condition that the SP approaches zero at infinite distance. Horizontal and bottom additional layers are adjoined to the model with the mesh width doubled every 5 elements to 6,350 m from both ends of the model, and for the thickness of 315 m, respectively. Zero SP values are assumed at the side and bottom

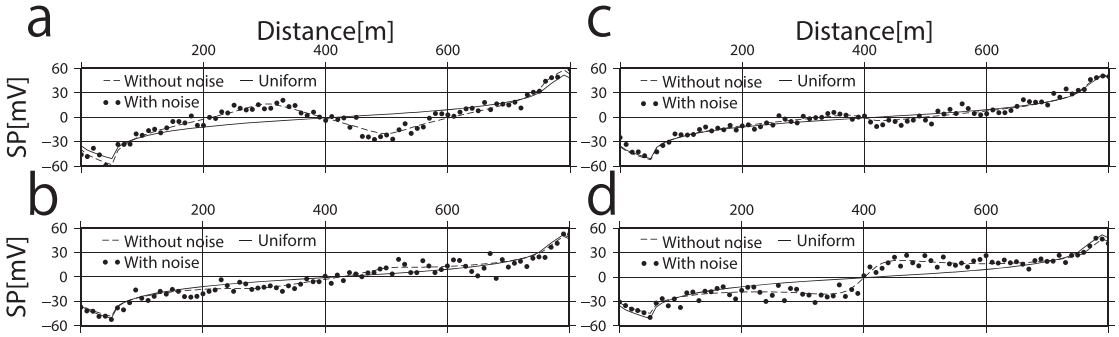

Figure 2. SP profile on the ground surface. The SP profile when the horizontal high (a) and low (b) permeability anomaly are buried. The SP profile when the vertical high (c) and low (d) permeability anomaly are buried. The solid lines show the SP profiles when the subsurface structure is uniform. The dashed lines show the SP profiles when the subsurface anomalies are buried. The dotted lines show the SP profiles for the inversion (the white noise with a deviation of 5 mV is added to the calculated input SP profiles).

boundaries of the SP model. The surface boundary condition for the SP calculation is set to no vertical current condition to represent the low conductivity of the air. In this study, we ignore the effect of groundwater flow in vadose zones on the SP profiles. We assume uniform values for the electrical conductivity (0.01 S/m) and streaming current coefficient (1.0×10^{-4} A/m^2). The background permeability is set to 1.0×10^{-6} m/s. The permeability of the imbedded anomalies is set to 1.0×10^{-4} m/s and 1.0×10^{-8} m/s.

SP Profile

Figure 2 shows SP profiles on the ground surface calculated from the models shown in Fig. 1. The dashed line in each plot shows the SP profile when the permeability anomaly is buried. The solid line shows the SP profile when the permeability structure is uniform. When the anomalous shape of permeability is horizontal (Figs. 2(a)–(b)), two peaks in the SP profiles appear at horizontal distances around 300 m and 500 m, just above the side boundaries of the permeability anomaly. On the basis of the distribution of the water head, we found that these anomalies are caused by the drastic change of the water head by the change in permeability. Two peaks caused by the high permeability anomaly (Fig. 2(a)) are higher than the two peaks caused by the low permeability anomaly (Fig. 2(b)). The peaks caused by the high permeability anomaly at 300 m and 500 m (dashed line in Fig. 2(a)) have an amplitude of about 23 mV, compared to the SP profile on the uniform permeability structure. On the other hand, the two peaks caused by the low permeability anomaly (dashed line in Fig. 2(b)) have smaller amplitudes of 8 mV. We found that the difference in groundwater flow pattern around the permeability anomaly affects the magnitude of the SP anomaly. The "lens effect" of the high permeability anomaly, which attracts the groundwater flow, increases the SP anomalies.

When the vertical permeability anomaly is buried (dashed line in Figs. 2(c)–(d)), the changes in the SP profiles appear from about 380 m to 420 m, just above the permeability anomaly. In this case, the low permeability anomaly (Fig. 2(d)) generates larger SP anomalies than the high permeability anomaly (Fig. 2(c)), contrary to the horizontal permeability anomaly case. The increment of the SP value from 380 m to 420 m is 26 mV (dashed line in Fig. 2(d)). On the other hand, the vertical high permeability anomaly does not change the SP profile greatly. The decrement of the SP profile from 380 m to 420 m is only 6.2 mV (dashed line in Fig. 2(c)); although a 1.8 mV increase is expected on the uniform structure model. This difference in magnitude of the SP anomalies is also caused by the different groundwater flow patterns around the permeability anomalies. In our models, the low vertical permeability anomaly interrupts the groundwater flow in the subsurface, resulting in the drastic water head changes around the low permeability anomaly. As a result, a large SP anomaly is generated by the low vertical permeability anomaly.

In the next section, we apply our inversion to these data as observed SP data. We evaluate how different SP responses caused by the permeability structures, especially the difference in magnitude of the SP anomalies caused by the permeability anomalies, affect the estimated permeability structure image obtained with our inversion scheme.

Inversion Result

The permeability structure was estimated according to the minimization of the objective function U described as Eq. (7). Because this inversion is a non-linear problem,

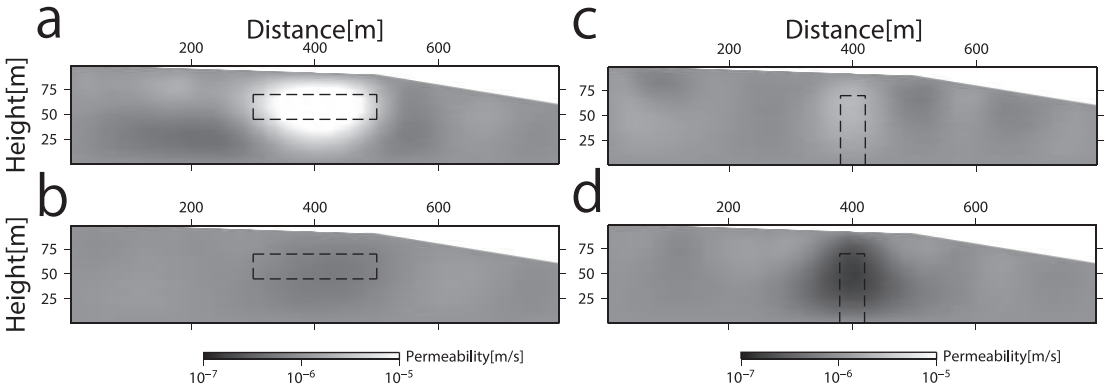

Figure 3. Overview of the inversion results. a), b), c) and d) are the inversion results from the noisy SP profiles in Figs. 2(a)–(d), respectively.

an iterative model modification process and an initial model are necessary. For the initial model, a uniform structure of permeability is used. As a priori information for the inversion, a uniform structure of the streaming current coefficient of 1.0×10^{-4} A/m^2 and electrical conductivity of 0.01 S/m are assigned. The inversion scheme includes a forward simulation of the groundwater flow and SP to calculate the error between the SP response from the estimated permeability structure and the input SP profile. The flux data of the groundwater flow at the recharge and discharge are necessary. The volume of the groundwater flow at the recharge and discharge, where the water heads are given to calculate the test data in the forward simulation, is also used as a priori data at each step in the inversion. The same meshes as the forward simulations are used for the calculation of the groundwater flow and SP during the inversion process.

Usually, the measured SP profile is contaminated by noise generated by factors other than groundwater flow. The oxidoreduction process (electro-redox contribution) caused by the corrosion of metallic materials in the subsurface also generates a SP field. Drift of the measuring electrodes caused by temperature changes is another source of noise. The temperature drift of the Pb/$PbCl_2$ electrode is 0.2 mV/°C (Rizzo *et al.,* 2004) and can be corrected with temperature data. The SP signals from oxidoreduction is larger than that from groundwater flow. For example, several hundred mV of SP fluctuations caused by the redox process (Naudet *et al.,* 2004) were observed in a landfill. Rizzo *et al.* (2004) removed the SP noise caused by the redox reaction and observed several mV of SP for the groundwater flow. This suggests that the noise level of SP for analyzing the groundwater flow can be reduced to several mV, therefore we added white noise with a deviation of 5 mV to the calculated SP profiles and input them as observed data.

Figure 3 shows the inversion results when the SP profiles shown in Fig. 2 are used as input data. The dashed lines show the exact location of permeability anomalies. The inversion process is terminated when the RMSE does not decrease or after five iterations. These results are obtained after five iterations of the model modification process. The final RMSE values are 1.5 mV, 1.8 mV, 1.2 mV and 1.6 mV for the noisy SP profiles in Figs. 2(a)–(d), respectively.

Inversion Result of Horizontal Anomalous Shape Case

When the input data are the SP profile affected by a horizontal high permeability anomaly, the high permeable area is reconstructed around the exact location of the permeability anomaly (Fig. 3(a)). The estimated high permeable area appears over a wider area than the true permeability anomalous area. The estimated high permeable zone starts from the vicinity of the ground surface. The shape of the estimated permeable zone is convex downward. This shape is influenced by the distribution of sensitivity of the SP response to the permeability of the initial model. The sensitivity decreases according to the depth from the ground surface. For the horizontal direction, the sensitivity becomes high around the center of the model (around 400 m along the horizontal axis in the plots). The image of the inversion result would follow the distribution of this sensitivity. In addition to the high permeability area, two artifacts of low permeability also appear at around 200 m and 500 m with a height of about 25 m. These artifacts appear after the third iteration when the maximum value of the estimated high permeable zone becomes larger than 3.5×10^{-5} m/s. We used a Laplacian smoothness operator for the inversion; these artifacts could be caused by the filtering operation.

When the input data are the SP profile affected by the horizontal low permeability anomaly, the low permeable anomaly rarely appears (Fig. 3(b)). The estimated low permeable area is smaller than the true permeability anomalous area, and its depth is deeper than the exact location of the permeability anomaly. The

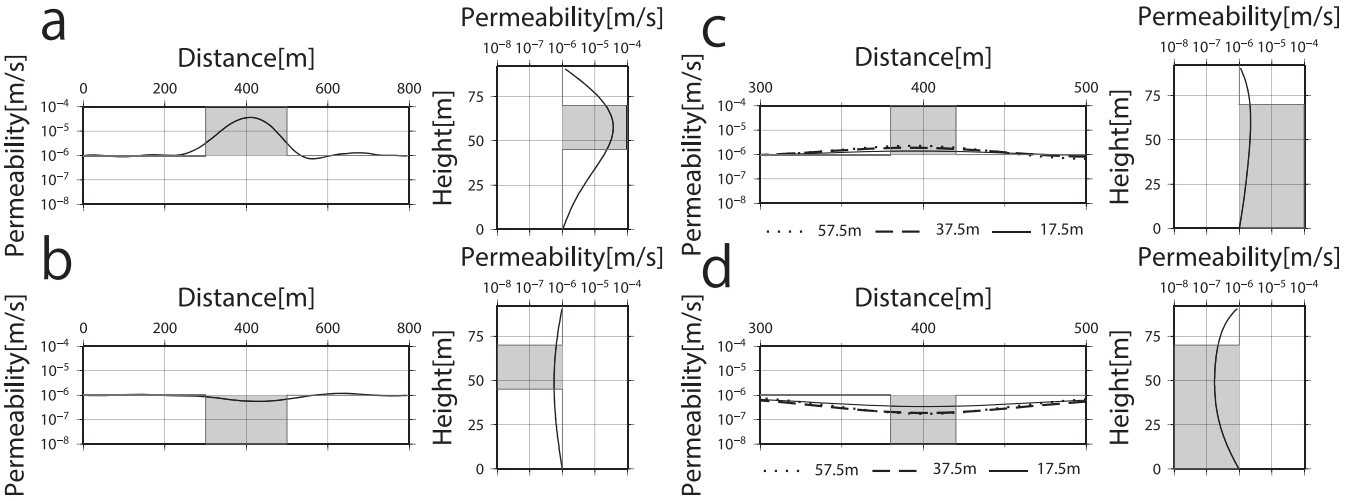

Figure 4. The horizontal (left graph in each subplot) and vertical (right graph in each subplot) variations of the estimated permeability. a) Shows the vertical variation at a horizontal location of 400 m and the horizontal variation at a height of 57.5 m of the estimated permeability in Fig. 3(a), and b) shows the vertical variation at a horizontal location of 400 m and the horizontal variation at a height of 57.5 m in Fig. 3(b). c) Shows the vertical variation at a horizontal location of 400 m and the horizontal variations at heights of 57.5 m, 37.5 m and 17.5 m in Fig. 3(c), and d) shows the vertical variation at a horizontal location of 400 m and the horizontal variation at heights of 57.5 m, 37.5 m and 17.5 m in Fig. 3(d).

contrast between the background and estimated permeability is also smaller than the true model and the contrast in the image of the high permeability anomaly case.

Inversion Result of Vertical Anomalous Shape Case

When the SP profile affected by the vertical high permeability anomaly is applied to the inversion, the high permeability anomaly appears only around the top boundary of the true permeability structure at a height of 70 m (Fig. 3(c)). The contrast in permeability between the high permeable image and background is much smaller than the true model.

When the SP profile affected by the vertical low permeability anomaly, which has a greater SP anomaly than the vertical high permeability anomaly, is used as input data, the estimated low permeability area appears around the true low permeable anomalous area (Fig. 3(d)). The estimated low permeability area is broader than the true low permeable anomalous area, and broadens with depth. This also is caused by the distribution of the sensitivity of SP response to the permeability, as with the case of the horizontal high permeability anomaly. In this case, the high permeability artifacts do not appear, even though the estimated lowest permeability is about ten times different from the background permeability.

Horizontal and Vertical Variation of Estimated Permeability

Figure 4(a) shows the horizontal variation of the estimated permeability at a height of 57.5 m, and the vertical variation at a horizontal distance of 400 m. Areas shaded grey are the location of the permeability anomaly. In this case, the highest estimated permeability becomes 3.6 $\times 10^{-5}$ m/s, almost half the value of the true permeability anomaly at a height of 57.5 m and a horizontal distance of 400 m. The horizontal location of the estimated high permeability area corresponds to the exact location of the permeability anomaly. The vertical variation of the estimated permeability anomaly is distributed not only inside the exact permeable zone, but also outside of it, owing to the smoothness constrain. However, the depth of the highest permeability in the estimated model is located within the true permeability anomalous area.

In the case of the horizontal low permeability anomaly, the lowest value of the estimated permeability is only 5.5×10^{-7} m/s at a height of 47.5 m and a horizontal distance of 455 m. Both the horizontal and vertical variations do not change much around the true permeability anomaly compared with other cases (Fig. 4(b)).

Figures 4(c)–(d) shows the horizontal and vertical variation of estimated permeability shown in Figs. 3(c)–(d). The vertical variation at a horizontal distance of 400 m and horizontal variations at heights of 57.5 m, 37.5 m and 17.5 m between the horizontal distance of 300 m and 500 m are shown with a dotted, dashed and solid line, respectively. In the case of the vertical high permeability anomaly, both the vertical and horizontal variation do not change much, although the permeability anomaly is 100 times higher than the surrounding material (Fig. 4(c)). The pattern of estimated permeability anomaly does not reconstruct the true permeability variation.

In the case of the vertical low permeability anomaly, all horizontal variations exhibit a lower permeability than the area surrounding the true permeable anomaly from 380 m to 420 m (Fig. 4(d)). The patterns of variation become sharper as the depth of the horizontal line becomes shallower. The lowest estimated permeability is 1.7×10^{-7} m/s and about ten times lower than the true permeability anomaly. In the vertical variation, the lowest permeability appears at a height of 48.5 m in the true permeability anomaly area. The low permeability area is widely distributed with depth, as with the estimated high permeability area, in the case of the horizontal high permeability anomaly (Fig. 4(a)).

We also tested the inversion under a noise-free condition. The inversion results for both the horizontal high and vertical low permeability anomalies are not much different from those with noise. The SP inversion would be robust for these detectable structures against noise. On the other hand, even if SP anomalies caused by the permeability anomaly are clearly seen in the noise-free condition, neither the horizontal low permeability anomaly nor the vertical high permeability anomaly could be detected. Estimation of the permeability anomaly that generates the small SP anomaly would be difficult by the SP inversion regardless of the noise level.

Effect of the Electrical Conductivity and Streaming Current Coefficient

The heterogeneity of the electrical conductivity and streaming current coefficient also affect the SP profile. The inversion is tested to evaluate how the heterogeneity of these parameters influence the inversion results. The electrical conductivity and streaming current coefficient are set to 0.1 S/m and 2.5×10^{-4} A/m^2, respectively, in the permeability anomaly of 1.0×10^{-4} m/s, and 0.001 S/m and 4.0×10^{-5} A/m^2, respectively, in the permeability anomaly of 1.0×10^{-8} m/s. The exact distribution of the electrical conductivity and streaming current coefficient are input to the inversion as a priori information. All inversion results show similar trends to the cases where heterogeneity of the electrical conductivity and streaming current coefficient were not considered. For the horizontal high and low permeability anomaly models, the estimated highest and lowest permeability are 1.1×10^{-5} m/s at a horizontal location of 395 m at a height of 50.5 m, and 2.9×10^{-7} m/s at a horizontal location of 385 m at a height of 49.5 m, respectively. For the vertical high and low anomaly cases, the high and low permeability estimates are 1.2×10^{-6} m/s at a horizontal location of 345 m at a height of 49.5 m, and 1.2×10^{-7} m/s at a horizontal location of 405 m at a height of 49.5 m, respectively.

Discussion

Our inversion results demonstrate that the inversion of SP data that are acquired on the ground surface can be used to evaluate permeability anomalies. The inversion is sensitive to permeability anomalies, in particular when horizontal high or vertical low permeability anomalies are present. In these cases, the SP profiles have a large SP deviation caused by the heterogeneity of a subsurface permeability structure. The permeability anomaly can be estimated correctly. In addition, these inversion results are robust to noise. As shown in Straface *et al.* (2011), SP measurements would help the estimation of permeability structure in the subsurface, especially for horizontal high or vertical low permeability structures.

On the other hand, the horizontal low permeability or vertical high permeability anomalies may not be well resolved with the inversion. Even for the noise-free cases, when the SP anomalies caused by the permeability anomalies are clearly seen, the permeability anomalies are not detectable. In these cases, the SP anomalies caused by the permeability anomalies are less than the SP anomalies caused by the horizontal high or vertical low permeability structure that are detectable by the inversion. Such a small SP anomaly could be generated by not only our given anomaly model, but also another small and lower contrast permeability anomaly structure. The permeability anomalies would not be imaged as the true model, but similar to the initial model because of the non-uniqueness of the inversion problem. Although the SP inversion could be robust for estimating permeability structures that exhibit large SP variations, the inversion may not reproduce the permeability structure for small SP signals that are caused by noise, the permeability anomaly, or both.

We also tested the effects of heterogeneity of the electrical conductivity and streaming current coefficient on the inversion for estimating the permeability structure. These parameters can affect the SP profile and should be considered in the SP inversion. The inversion results show similar trends to those without the heterogeneities (when these parameters are given as a priori data). This proves the feasibility of the SP measurement to estimate the permeability structure when provided the values of the electrical conductivity and streaming current coefficient, even though the SP is affected by these parameters. The estimated electrical conductivity structure is available if the DC or EM measurement is conducted with the SP measurement. The estimated electrical conductivity structure from other geophysical methods, for example DC resistivity soundings or electromagnetic methods, will help with the construction of the optimal a priori data. Recently, the relationship between permeability and streaming

current coefficient was observed (*e.g.,* Jardani and Revil, 2009), and could be used to reduce the number of unknown model parameters.

Conclusions

In this study, we developed an inversion algorithm for the estimation of permeability anomaly from a SP profile and subsurface permeability structure from water head data. The synthetic SP profiles show that the deviation of a SP profile caused by a subsurface permeability anomaly depends on both the shape and the value of the permeability anomalies. Our inversion results indicate that the SP inversion can produce a more accurate image of the permeability structure when the SP signal caused by the permeability anomaly is large. The regional groundwater flow pattern around the zone of permeability anomalies can control the shape and magnitude of the generated SP anomaly; therefore, the flow pattern in the subsurface needs to be considered in the analysis of SP anomalies.

References

Fournier, C., 1989, Spontaneous potentials and resistivity surveys applied to hydrogeology in a volcanic area: Case history of the Chaîne des Puys (Puy-de-Dôme, France): Geophysical Prospecting, **37**, 647–668, doi: 10.1111/j.1365-2478.1989.tb02228.x.

Ishido, T., and Pritchett, J.W., 1999, Numerical simulation of electrokinetic potentials associated with subsurface fluid flow: J. Geophys. Res., **104**(B7) 15247–15259, doi:10.1029/1999JB900093.

Jardani, A., Revil, A., Barrash, W., Crespy, A., Rizzo, E., Straface, S., Cardiff, M., Malama, B., Miller, C., and Johnson, T., 2009, Reconstruction of the water table from self-potential data: A Bayesian approach: Ground Water, **47**, 213–227, doi: 10.1111/j.1745-6584.2008.00513.x.

Jardani, A., and Revil, A., 2009, Stochastic joint inversion of temperature and self-potential data: Geophys. J. Int., **179**, 640–654, doi: 10.1111/j.1365-246X.2009.04295.x.

Naudet, V., Revil, A., Rizzo, E., Bottero, J.Y., and Bégassat, P., 2004, Groundwater redox conditions and conductivity in a contaminant plume from geoelectrical investigations: Hydrol. Earth. Syst. Sci., **8**, 8–22, doi:10.5194/hess-8-8-2004.

Ozaki, Y., Mikada, H., Goto, T., and Takekawa, J., 2012, Effects of subsurface permeability structure on self potential distribution: *in* Expanded Abstracts: 82nd Annual International Meeting, Society of Exploration Geophysics, doi: 10.1190/segam2012-1117.1.

Revil, A., Naudet, V., Nouzaret, J., and Pessel, M., 2003, Principles of electrography applied to self-potential electrokinetic sources and hydrogeological applications: Water Resour. Res., **39**, 1114, doi:10.1029/2001WR000916.

Revil, A., Naudet, V., and Meunier, J.D., 2004, The hydroelectric problem of porous rocks: Inversion of the position of the water table from self-potential data: Geophys. J. Int., **159**, 435–444, doi: 10.1111/j.1365-246X.2004.02422.x.

Revil, A., and Jardani, A., 2010, Stochastic inversion of permeability and dispersivities from time lapse self-potential measurements: A controlled sandbox study: Geophys Res. Lett., **37**, L11404, doi: 10.1029/2010GL043257.

Rizzo, E., Suski, B., Revil, A., Straface, S., and Troisi, S., 2004, Self-potential signals associated with pumping tests experiments: J. Geophys. Res., **109**, B10203, doi:10.1029/2004JB00304.

Sheffer, M.R., 2007, Forward modeling and inversion of streaming potential for the interpretation of hydraulic conditions from self-potential data, Ph.D. thesis, The University of British Columbia, Vancouver, British Columbia, Canada.

Sill, W., 1983, Self-potential modeling from primary flows: Geophysics, **48**(1) 76–86, doi: 10.1190/1.1441409.

Straface, S., Chidichimo, F., Rizzo, E., Riva, M., Barrash, W., Revil, A., Cardiff, M., and Guadagnini, A., 2011, Joint inversion of steady-state hydrologic and self-potential data for 3D hydraulic conductivity distribution at the Boise Hydrogeophysical research site: J. Hydrol., **407**, 115–128, doi: 10.1016/jhydrol.2011.07.013.

Titov, K., Ilyin, Y., Konosavski, P., and Levitski, A., 2002, Electrokinetic spontaneous polarization in porous media: Petrophysics and numerical modeling: J. Hydrol., **267**, 207–216, doi: 10.1016/S0022-1694(02)00151-8.

Uchida, T., 1993, Smooth 2-D inversion for magnetotelluric data based on statistical criterion ABIC: J. Geomagn. and Geoelectr., **45**, 841–858.